International Journal of Precision Engineering and Manufacturing-Green Technology
https://doi.org/10.1007/s40684-021-00319-6

Online ISSN 2198-0810
Print ISSN 2288-6206

REGULAR PAPER

Porosity Evaluation of Additively Manufactured Components Using Deep Learning-based Ultrasonic Nondestructive Testing

Seong-Hyun Park[1] · Sungho Choi[2] · Kyung-Young Jhang[3]

Received: 17 June 2020 / Revised: 20 January 2021 / Accepted: 2 February 2021

Abstract
This study proposed deep learning-based ultrasonic nondestructive testing for porosity evaluation of additively manufactured components. First, porosity mechanisms according to additive manufacturing (AM) processing conditions were studied using traditional scanning acoustic microscopy and optical microscopy. Second, correlations between ultrasonic properties and porosity content were analyzed. The correlation results showed that the increased porosity content resulted in a decreased ultrasonic velocity and increased ultrasonic attenuation coefficient. Third, various levels of porosities were evaluated using a deep learning model based on a fully connected deep neural network that was trained on raw ultrasonic signals measured in the AM samples. After training, the testing performance of the trained model was evaluated. Additionally, the generalization performance of the pre-trained model was assessed using newly fabricated AM samples that were not used for training. The results showed that the porosity content evaluated by the pre-trained model matched well with that measured via traditional scanning acoustic microscopy, thus demonstrating the feasibility of deep learning-based ultrasonic nondestructive testing for porosity evaluation of additively manufactured components.

Keywords Additive manufacturing · Porosity · Ultrasonic nondestructive testing · Deep learning

1 Introduction

Additive manufacturing (AM), which can be more effectively used to produce innovative, complex, and lightweight products than conventional casting or subtractive manufacturing methods, has been actively studied in various fields [1–3]. One of the current issues is evaluating manufacturing defects that can occur during the AM process. Porosity is a typical manufacturing defect that can occur inside AM components due to non-optimal AM processing conditions [4]. Since its presence seriously affects the mechanical properties of AM components, evaluating the porosity through nondestructive testing (NDT) is essential [5].

Ultrasonic testing is an NDT method that can effectively evaluate porosity in materials [6–9]. In this testing, ultrasonic parameters, including the ultrasonic velocity and ultrasonic attenuation coefficient, are generally measured and correlated with porosity content [10]. These parameters are also related to mechanical properties influenced by porosity, such as elastic modulus, material density, and strength [11–13]. The correlation between ultrasonic velocity and porosity content in AM components was studied by Slotwinski et al. [14]. They correlated the ultrasonic velocity with the porosity content results measured by bulk mass measurements, Archimedes measurements, and X-ray computed tomography. The measured ultrasonic velocity was inversely related to the porosity content. Karthik et al. [10] investigated the correlation between ultrasonic parameters and material properties of AM components. The ultrasonic velocity and ultrasonic attenuation coefficient were measured using a water immersion method, and the ultrasonic

✉ Sungho Choi
schoi@jbnu.ac.kr

✉ Kyung-Young Jhang
kyjhang@hanyang.ac.kr

[1] Department of Mechanical Convergence Engineering, Hanyang University, 222 Wangsimni-ro, Seongdong-gu, Seoul 04763, Republic of Korea

[2] Department of Flexible and Printable Electronics, LANL-JBNU Engineering Institute-Korea, Jeonbuk National University, 567 Baekje-daero, Deokjin-gu, Jeonju-si, Jeollabuk-do 54896, Republic of Korea

[3] School of Mechanical Engineering, Hanyang University, 222 Wangsimni-ro, Seongdong-gu, Seoul 04763, Republic of Korea

Published online: 19 April 2021

results were correlated with material properties, including material density and grain size. They reported that the ultrasonic velocity was highly correlated with material density, which can be affected by porosity content. These previous experimental studies demonstrated that ultrasonic testing can be effectively used to evaluate porosity content in AM components.

In recent years, deep learning using neural networks has been rapidly developing [15, 16], and applying deep learning methods to ultrasonic testing is of great interest [17, 18]. One significant benefit of the deep learning method is that it provides an excellent ability to accurately and consistently interpret ultrasonic signals for detection and characterization of defects [19], while conventional ultrasonic pattern recognition [20] is error-prone and usually depends on the experience and knowledge of inspectors. Moreover, deep learning provides automatic ultrasonic signal classification according to the defect type and damage severity [21, 22]. Several studies have reported on the application of deep learning methods to ultrasonic testing for the detection of cracks [23, 24], corrosion [25], weldment defects [26], and others [22, 27] in metals and composite materials. However, deep learning-based ultrasonic testing for inspection of AM components has rarely been investigated.

In this work, ultrasonic NDT with deep learning was applied for porosity evaluation of AM components. First, porosity mechanisms according to varying AM processing conditions were investigated using traditional scanning acoustic microscopy and optical microscopy. Second, correlations between ultrasonic parameters and porosity content in AM components were analyzed. AM samples containing various levels of porosity content were fabricated, and the amounts of porosity in the samples were quantified by scanning acoustic microscopy. Ultrasonic velocity and ultrasonic attenuation coefficients were measured using a pulse-echo method. After the fundamental analysis of this correlation, a deep learning model for porosity evaluation of AM components was developed based on a fully connected deep neural network. This deep learning model was trained on time-domain ultrasonic signals obtained from the AM samples, where the samples were categorized into six classes according to the quantitative amount of porosity content. Then the testing performance of the trained model was evaluated. Additionally, the generalization performance of the pre-trained model was assessed using newly fabricated AM samples that were not used for the training.

2 Correlation Between Ultrasonic Parameters and Porosity Content in AM Components

2.1 Experimental Procedures

AM samples containing various levels of porosity content were fabricated under various AM processing conditions. A selective laser melting machine (SLM 280 2.0; SLM Solutions, Germany) was used with Ti powder with 20–63 μm particle diameters. The AM processing variables considered were the laser power and laser scan speed, which were related to laser energy density. Three different laser powers of 235, 275, and 315 W were used. At each power, the laser energy density varied from 55 to 90 J/mm^3 in 5 J/mm^3 increments by adjusting the laser scan speed. The hatch space and layer thickness were fixed at 0.12 mm and 0.03 mm, respectively. The variations of those processing parameters are closely related to porosity generation mechanisms [28, 29]. After AM processing, the top and bottom surfaces of the samples were surface-processed by wire electrical discharge machining. Each sample was $20 \times 20 \times 2.8$ mm^3 in size. Twenty-four AM samples fabricated under different processing conditions are shown in Fig. 1. Each sample is numbered from #1 to #24. The AM processing conditions considered are described in Table 1.

Quantitative amounts of porosity contained in the fabricated AM samples were assessed via traditional scanning acoustic microscopy in a water-immersion mode. Ultrasonic C-scan was performed using a scanning acoustic microscope

Fig. 1 Twenty-four AM samples fabricated under different processing conditions. Each sample is numbered from #1 to #24

Table 1 The AM processing conditions used to manufacture the test samples

	Sample name							
	#1	#2	#3	#4	#5	#6	#7	#8
Laser power (W)	315	315	315	315	315	315	315	315
Scan speed (mm/s)	1590	1460	1350	1250	1170	1090	1030	970
Laser energy density (J/mm^3)	55	60	65	70	75	80	85	90
	Sample name							
	#9	#10	#11	#12	#13	#14	#15	#16
Laser power (W)	275	275	275	275	275	275	275	275
Scan speed (mm/s)	1390	1270	1170	1090	1020	950	900	850
Laser energy density (J/mm^3)	55	60	65	70	75	80	85	90
	Sample name							
	#17	#18	#19	#20	#21	#22	#23	#24
Laser power (W)	235	235	235	235	235	235	235	235
Scan speed (mm/s)	1190	1090	1000	930	870	820	770	720
Laser energy density (J/mm^3)	55	60	65	70	75	80	85	90

(HS-1000; Sonix, USA) with a 75 MHz focusing-type transducer. This scanning acoustic microscopy provided an in-plane spatial resolution of 80 µm. The transducer's focal point and the C-scan gate were located in the middle of the sample in the thickness direction. The gate width was 1.4 mm, which corresponded to half the sample thickness, and the comprehensive results for porosity that existed in the half region were evaluated.

Ultrasonic measurements for the ultrasonic velocity and ultrasonic attenuation coefficient were based on a pulse-echo method using a contact transducer, which uses a broad-band pulsed signal and multiple unrectified back-wall echoes [30]. A schematic diagram and the experimental setup are shown in Fig. 2. An electric spike pulsed signal provided by a pulser/receiver (PR5072; Panametrics, USA) was sent to a 10 MHz piezoelectric transducer. The transducer is one of the commercially available contact transducers that provides a relatively high frequency. This high frequency was chosen to induce the ultrasonic attenuation and scattering effects caused by pores as much as possible. The transducer excited a longitudinal wave of approximately 600 µm wavelength into the AM sample and received back-wall echoes. The received echoes reflect the influence of all pores in the ultrasonic propagation path in the form of changes in the ultrasonic velocity and attenuation coefficient. At this ultrasonic wavelength condition, the ultrasonic diffraction effect is small enough to be ignored because all samples have the same thickness of 2.8 mm and the wave propagation distance is within the range of Fresnel zone, which is calculated by $D^2/4\lambda = 37$ mm, where D is the transducer diameter and λ is the wavelength [31]. The contact pressure between the transducer and the sample was maintained consistently in each measurement by using a pneumatic system

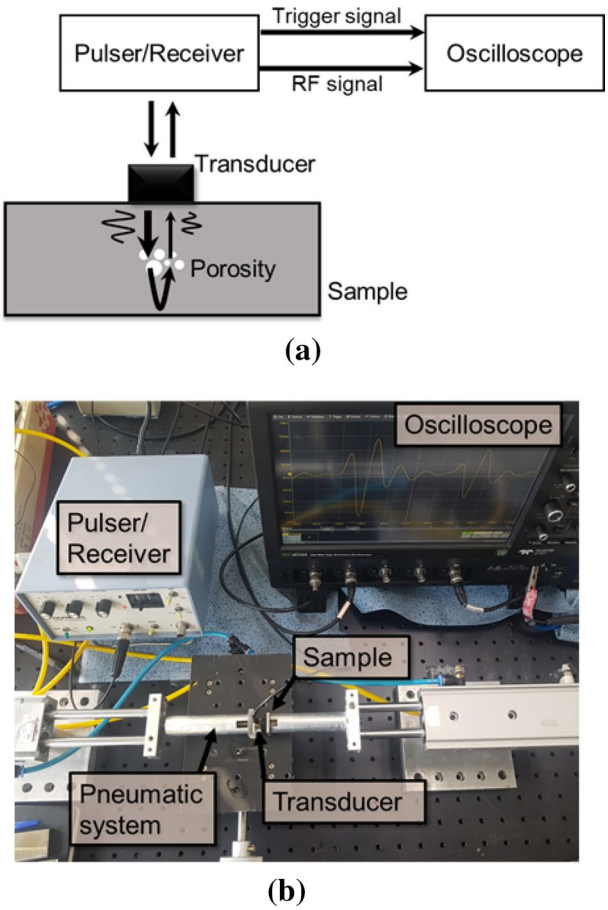

Fig. 2 **a** Schematic diagram, and **b** a picture of the experimental setup for ultrasonic velocity and ultrasonic attenuation coefficient measurements

Table 2 Conditions for the ultrasonic wave and filter

Frequency	Wavelength	Filter (Cutoff frequency)
10 MHz	600 μm	High pass filter (1 MHz)

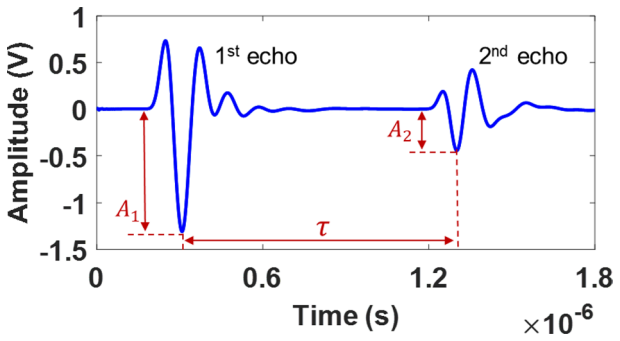

Fig. 3 Typical ultrasonic echo signal used for the measurements of ultrasonic velocity and attenuation coefficient

to minimize the measurement errors [32, 33], as shown in Fig. 2b. The received ultrasonic signals were high-pass filtered with a cutoff frequency of 1 MHz to remove background noise and recorded on an oscilloscope (HDO4034A; Teledyne LeCroy, USA). The ultrasonic frequency, wavelength, and the used filter are provided in Table 2.

Ultrasonic velocity was calculated from the time-of-flight (TOF) between the first and second back-wall echoes (as shown in Fig. 3) and the sample thickness, using the following relationship [30]:

$$v = \frac{2d}{\tau}, \tag{1}$$

where v, d, and τ are the ultrasonic velocity, the sample thickness, and the TOF between the first and second back-wall echoes, respectively. The ultrasonic attenuation coefficient was calculated from the following equation [34]:

$$a = \frac{20}{2d} log\left(\frac{A_1}{A_2}\right), \tag{2}$$

where α is the ultrasonic attenuation coefficient, and A_1 and A_2 are the amplitudes of the first and second back-wall echoes, respectively.

2.2 Experimental Results and Discussion

Typical C-scan images of AM samples fabricated under various AM processing conditions are shown in Fig. 4. It is clearly observed that bright spots representing the presence of internal porosity are distributed differently according to the AM processing variables. From these C-scan images, the quantitative amounts of porosity content were calculated by using the 2D image analysis software ImageJ [35]. The C-scan images were processed to binarization using the 6 dB drop method, and then the porosity content was determined as the ratio of the porous area that appears as bright spots to the total area.

The porosity contents evaluated from the C-scan images are shown in Fig. 5. To observe the type of porosity according to the porosity formation mechanism, optical microscopy was also used for the #1 and # 24 samples, as shown in Fig. 6. When the laser power was 315 W, as the laser energy density became lower than 65 J/mm^3 a sharp increase in porosity content was observed, as shown in Fig. 5a. This was because an increase in laser scan speed caused the lack of laser energy in the melt pool, and the insufficient energy caused lack of fusion (LOF) of the Ti powder in inter and/or intra layers of the AM components. This type of porosity was generally observed with unfused particles, as shown in Fig. 6a [36], and called LOF porosity. On the other hand,

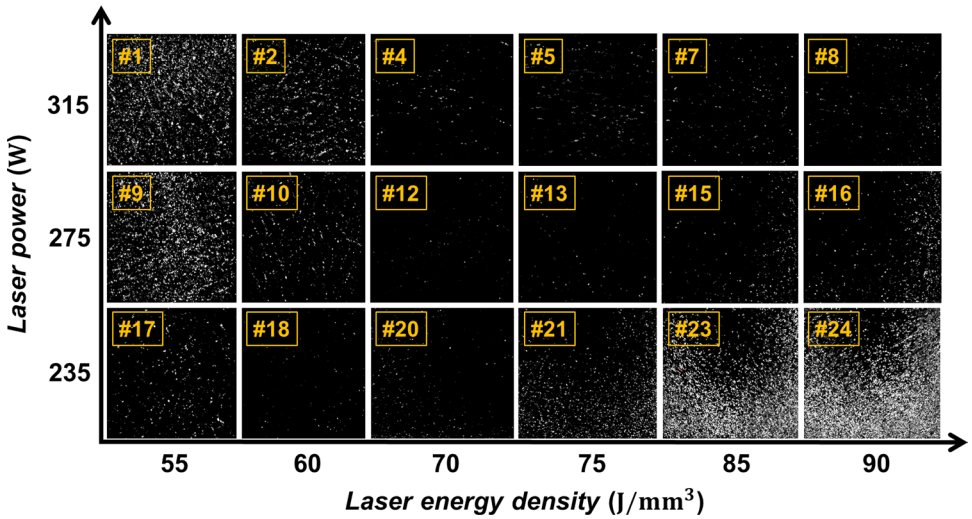

Fig. 4 Typical C-scan images of AM samples fabricated under various AM processing conditions

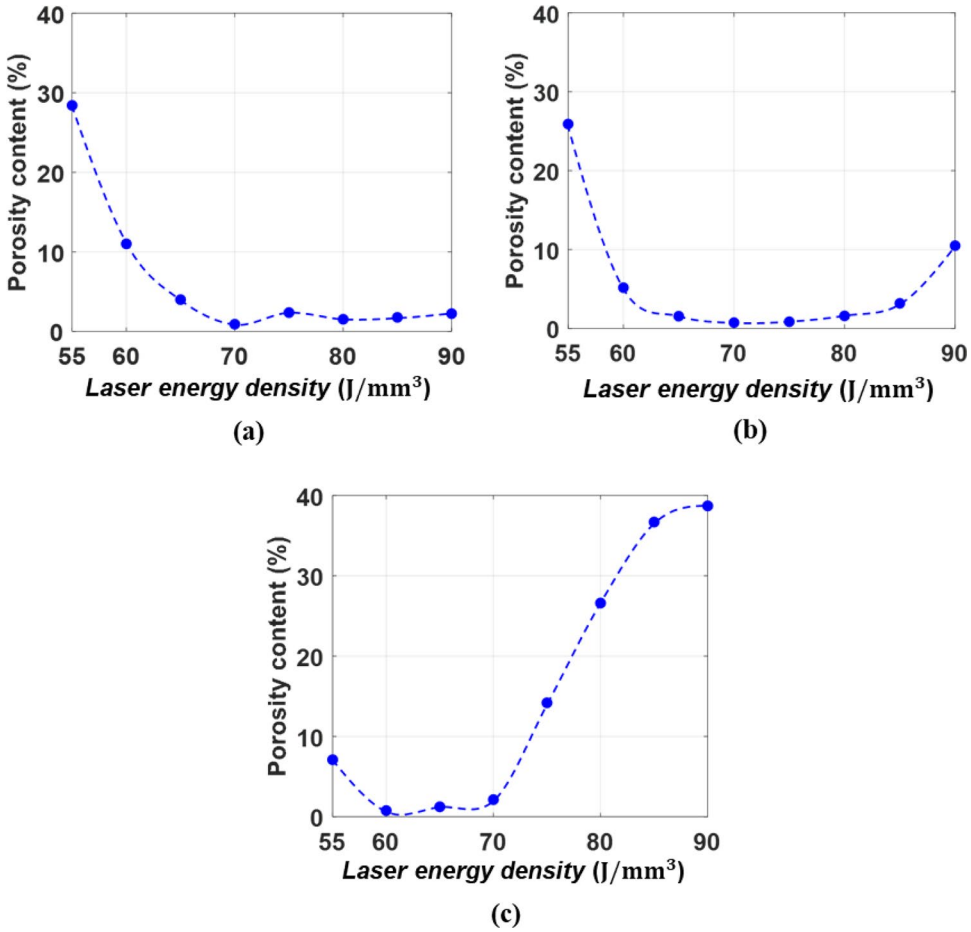

Fig. 5 The quantitative amounts of porosity content evaluated from the C-scan images at laser powers of **a** 315 W, **b** 275 W, and **c** 235 W

when the laser energy density was greater than 70 J/mm^3, the porosity content was quite low, about 2–3%. At a laser power of 275 W, the threshold laser energy density for LOF slightly decreased, shifted to 60 J/mm^3, as shown in Fig. 5b. Conversely, the porosity content increased rapidly as the laser energy density increased above 85 J/mm^3. In contrast to the previous case, the main cause was because a decrease in laser scan speed caused excessive laser energy in the melt pool, which resulted in welded particles and wavy surfaces as well as an increase in gas solubility. As the printing path of the powder recoating blade interfered with the welded particles and wavy surfaces of the previous layer, the small pit-shape porosity occurred. Besides, an increase in entrapped gas owing to an increase in gas solubility caused the change in gas porosity [37, 38], as shown in Fig. 6b. When the laser power was 235 W, the threshold laser energy density for over-melting was shifted to 70 J/mm^3, as shown in Fig. 5c. These results indicate that porosity is interrelated with the varying AM processing conditions and can be caused by various generation mechanisms. Therefore, efforts for porosity evaluation through NDT are required.

The quantitative amounts of porosity content evaluated via traditional scanning acoustic microscopy were correlated with the ultrasonic velocity and ultrasonic attenuation coefficient obtained using ultrasonic measurements. The relationship between ultrasonic velocity and porosity content is shown in Fig. 7, where the ultrasonic velocity is represented from the average value of ten measurements and the average deviation of repeated measurements for each sample was within 0.03%. Overall, the ultrasonic velocity was inversely related to the porosity content. A decrease in ultrasonic velocity up to 0.6% is observed in the samples in which the LOF and over-melting porosities were measured. This inverse-proportional relationship resulted from the ultrasonic velocity being proportional to the mechanical properties, including density and stiffness, whereas the presence of porosity caused degradation of the mechanical properties [39, 40]. Figure 8 shows the relationship between the ultrasonic attenuation coefficient and porosity content. Similarly with the ultrasonic velocity measurement, the measured values were averages of ten measurements and the average deviation of repeated measurements was within 3%. In contrast to the ultrasonic velocity, there was a proportional relationship between the ultrasonic attenuation coefficient and porosity content. An increased attenuation coefficient up to 26% is observed in the sample with porosity compared to that of the porosity-free sample. This was because ultrasonic

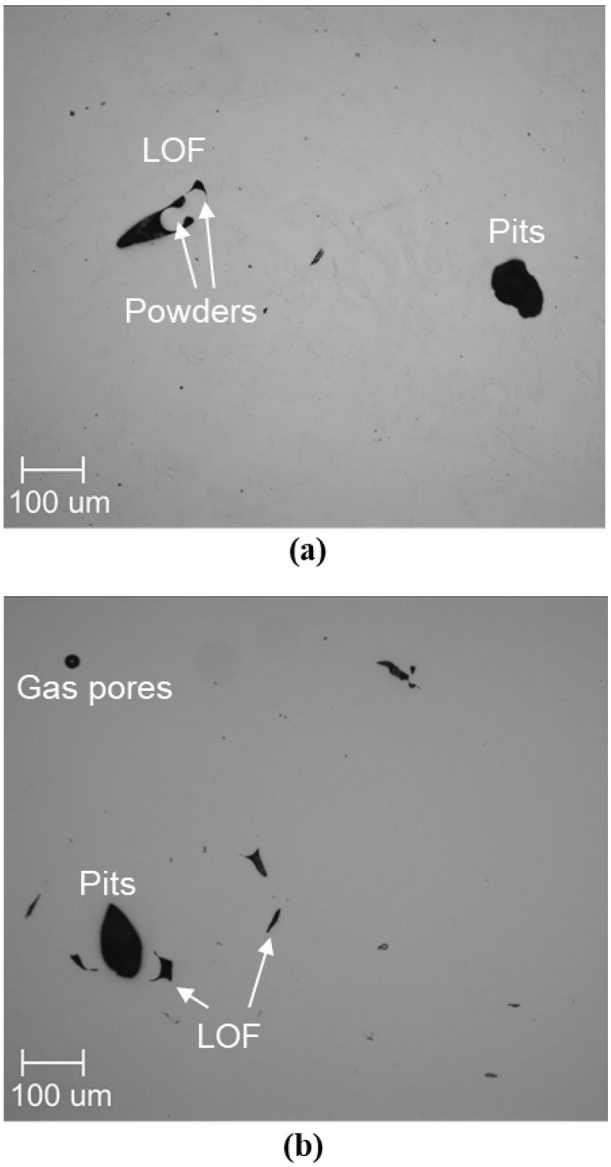

Fig. 6 The optical microscopy images for **a** the #1 and **b** #24 samples

waves were scattered at the boundaries of pores during the wave propagation. The larger the number of pores, the more attenuation of ultrasonic waves [41]. These ultrasonic results demonstrate that the use of ultrasonic NDT using ultrasonic velocity and attenuation coefficient measurements can effectively assess the porosity of AM components.

3 Porosity Evaluation using Deep learning-based Ultrasonic Testing

3.1 Structure of the Deep Learning Model

Artificial neural networks are statistical machine learning algorithms, of which concept was manifested by Rosenblatt's perceptron in 1958, which was inspired by biological neurons [42]. The simplest model is a single-hidden-layer feedforward neural network, which is composed of three layers: an input layer, a hidden layer, and an output layer. Every node in each layer is related to a respective node in the previous layer and has a characteristic weight. In ultrasonic testing, a fully connected deep neural network (DNN) and a convolutional neural network (CNN) are commonly used according to a signal-to-noise ratio (SNR) condition for the ultrasonic signal [22, 43]. Generally, a DNN, composed of two or more hidden layers with the input and output layer, is a better choice for high SNR condition due to its architectural simplicity. A CNN, composed of convolutional and pooling layers with the fully connected DNN, is known to be effective for low SNR condition. In this work, a fully connected DNN consisting of two hidden layers was adopted for the deep learning-based ultrasonic testing model because the SNR level of the ultrasonic signal used for training and testing the model is relatively high, achieving a value of 33 dB.

An architecture of the deep learning model is shown in Fig. 9. The number of nodes in an input layer and an output layer was set to 6000 and 6, respectively. After several trials were run, the number of nodes in each hidden layer was set to 1000, which was determined to be the optimal value that resulted in the best performance versus training time. Additionally, to avoid an overfitting problem, a dropout regularization method with a training probability of 70% was applied in each layer. Among several classification functions, a rectified linear unit (ReLU) was used as an activation function; this is generally utilized in a fully connected DNN. A softmax cross-entropy function was used to calculate the error and to improve the classification accuracy in deep learning [44]. The learning rate was set to 0.005, which was determined to be independent of overfitting after several trials were run. DNN parameters are denoted in Table 3. This deep learning model was designed using Google TensorFlow and Keras.

3.2 Training and Testing of Deep Learning Model

The deep learning model was trained using a classification in supervised learning, which is a machine learning method used to derive a specific function from the training

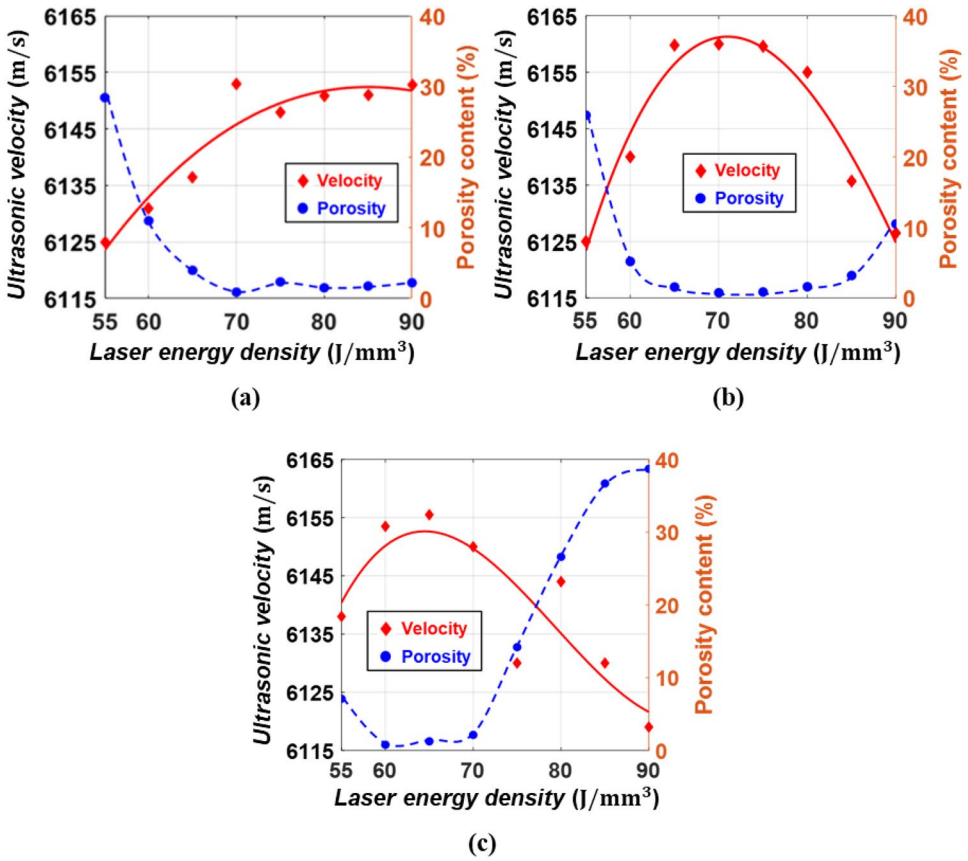

Fig. 7 The relationship between ultrasonic velocity and porosity content at laser powers of **a** 315 W, **b** 275 W, and **c** 235 W

data, and then the performance of the trained model was evaluated. For classification, the respective training data should have a class label as an output. In this work, AM samples were divided into six classes labeled with porosity level 0, 1, 2, 3, 4, and 5, based on the results of porosity content evaluated by traditional scanning acoustic microscopy, as shown in Table 4. The number of these classes corresponded to the number of outputs in the DNN model shown in Fig. 9. Raw ultrasonic echo signals, which were used to obtain ultrasonic parameters, were also utilized as data to train the deep learning model. The sampling number of those signals was 6,000, corresponding to the number of input nodes. For each class, 500 ultrasonic signals were acquired from the AM samples, where 400 signals were extracted randomly and used for training data. The remaining 100 signals were used for testing data. Considering the previous studies, the amount of data used for the training and testing of the model is reasonably sufficient [23]. The details of the training and testing database are summarized in Table 4.

The training accuracy of the deep learning model according to the iteration number is shown in Fig. 10. The training accuracy represents the classification performance at each iteration for the training data and was calculated as:

$$Training \quad accuracy = \frac{m_{Training}}{n_{Training}} \times 100, \tag{3}$$

where $m_{Training}$ is the number of training data classified correctly and $n_{Training}$ is the total number of training data. The training accuracy started at 16% and gradually improved as the iteration number increased. The accuracy reached 100% for the first time at the 775th iteration number and then it became stable. A stable training accuracy means that the model has a global minimum cost. Thus, the learning process was terminated after 1,000 iterations. The training procedure was conducted using a commercial CPU device and its total computation time was about 500 s.

After the training, the testing accuracy of the trained model was evaluated. The results are summarized in Table 5, where the testing accuracy for each class was calculated as:

$$Testing \quad accuracy = \frac{m_{Testing,i}}{n_{Testing,i}} \times 100 (i = 0{-}5), \tag{4}$$

where $m_{Testing,i}$ is the number of testing data classified correctly from the class i, and $n_{Testing,i}$ is the total number of testing data from the class i. The average testing accuracy for all classes was 93%. Especially, for classes above porosity level 2, the testing accuracy was over 95%. According to

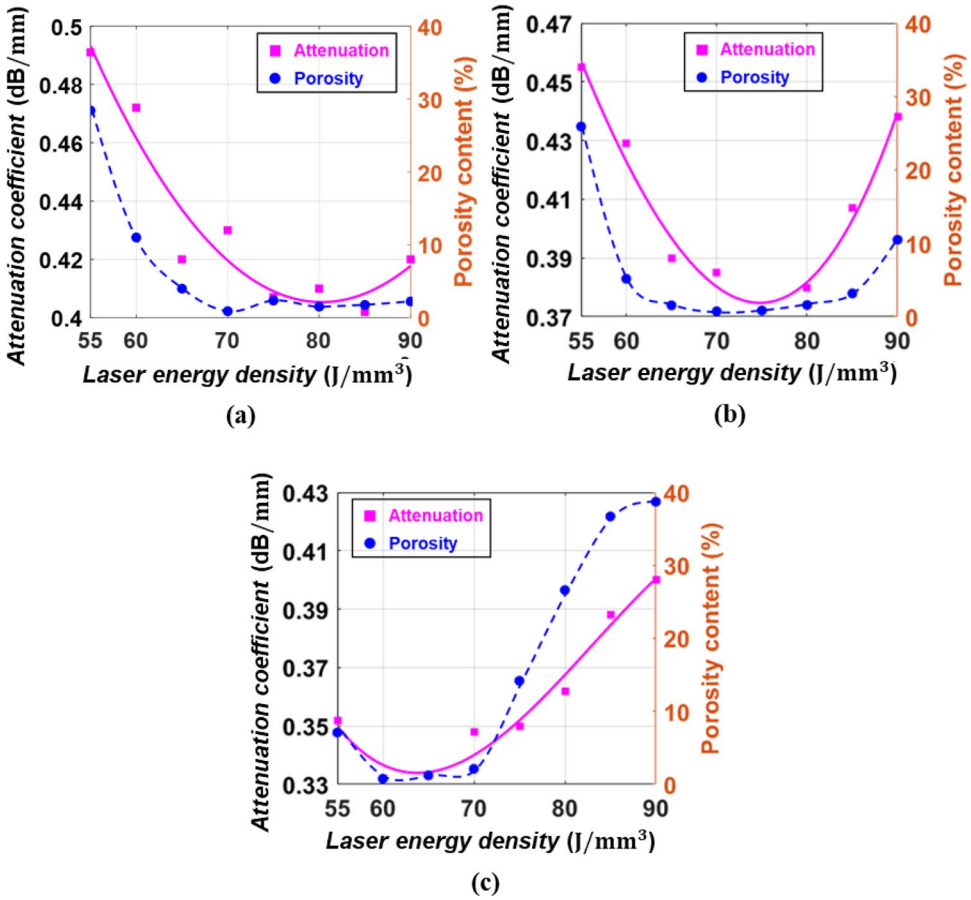

Fig. 8 The relationship between ultrasonic attenuation coefficient and porosity content at laser powers of **a** 315 W, **b** 275 W, and **c** 235 W

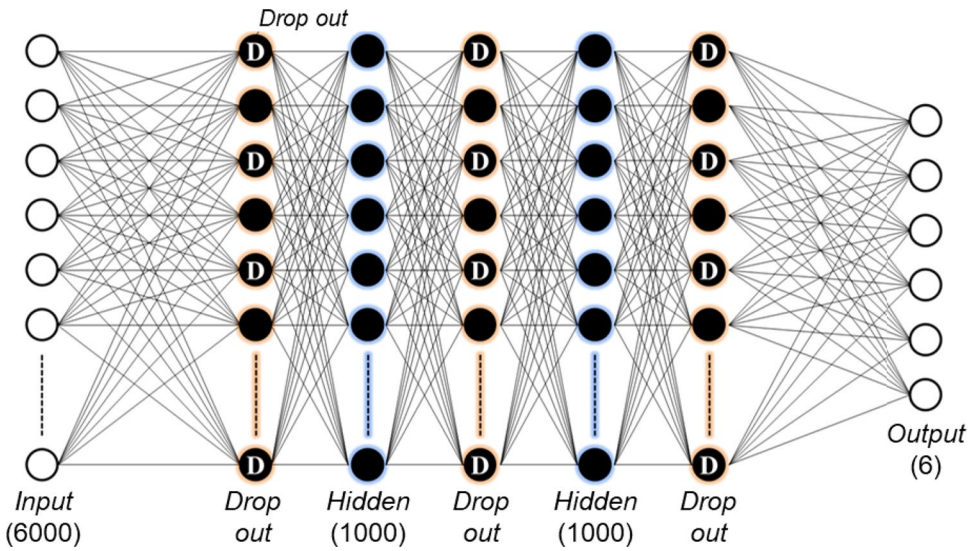

Fig. 9 Architecture of the fully connected DNN model

Table 3 DNN parameters used for model training

Layer type	Input layer	Fully connected layer (Wide)	Fully connected layer (Deep)	Drop out	Learning rate	Cost function	Activation function
Size	6000	1000	2	70%	0.005	Softmax cross-entropy	ReLU

Table 4 Training and testing database

Classification	Porosity content (%)	AM sample	Number of ultrasonic signals	
			For training	For testing
Level 5	More than 28	#23, #24	400	100
Level 4	24–28	#1, #9, #22	400	100
Level 3	12–16	#21	400	100
Level 2	8–12	#2, #16	400	100
Level 1	4–8	#10, #17	400	100
Level 0	0–4	#3, #4, #5, #6, #7, #8, #11, #12, #13, #14, #15, #18, #19, #20	400	100

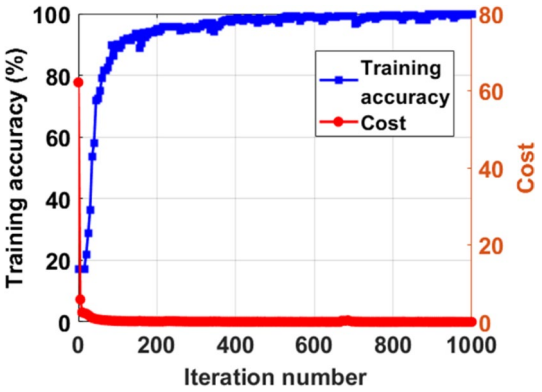

Fig. 10 The training accuracy and cost of the deep learning model according to the iteration number

the results of correlation studies between the porosity and ultrasonic properties, there was a delay in arrival time of ultrasonic waves and also an amplitude loss owing to the ultrasonic scattering of ultrasonic waves propagating in a porous medium. Those effects changed the waveforms of the raw ultrasonic signals, which were extracted as features during model training. This process allows the deep learning model to evaluate the porosity with a raw ultrasonic signal.

Meanwhile, orthotropic properties of the AM material may also affect the performance of the deep learning-based ultrasonic testing, depending on the measurement position. Generally, AM material has a strong anisotropic orientation along the AM building direction due to the non-uniformity of porosity. However, there is relative uniformity on the plane parallel to the surface in contact with the transducer in our experiments [45]. In other words, the distribution of pores perpendicular to the surface in contact with the transducer (that is, the direction of the AM building) may be non-uniform, but the average pore along this direction is mostly uniform in the direction horizontal to the surface. In our experiments, ultrasonic waves propagate in a direction perpendicular to the surface, and the received signal reflects the influence of all pores along this path. Further, the degree of this influence does not change significantly even if the position of the transducer is changed, so there may be few errors in the performance owing to orthotropic issues in our experiments. Nevertheless, to minimize the error factor due to the different measurement positions, each ultrasonic signal used for model training was measured with slightly varying measurement positions. This resulted in the performance being independent of the measurement position above porosity level 2. However, those assumptions might be difficult to establish in the case of small amounts of porosity content. In fact, our experimental results showed a slightly lower accuracy of 82% and 86% for classes of porosity levels 0 and 1 compared to the other classes. This low accuracy also results from very small changes in the ultrasonic waves due to less porosity and the experimental noise. When the porosity content is very low, the changes in ultrasonic waves are also very small, so ultrasonic measurements are significantly affected by the experimental noise. For low porosity content, these experimental limits are inevitable.

Note that the wave propagation direction was the same as the AM building direction in our experiments. However,

Table 5 Confusion matrix for the testing accuracy of the trained model

Unit: %	Level 0	Level 1	Level 2	Level 3	Level 4	Level 5
Level 0	82	12	4	1	1	0
Level 1	11	86	2	1	0	0
Level 2	1	1	98	0	0	0
Level 3	0	0	0	100	0	0
Level 4	0	0	0	0	99	1
Level 5	0	1	0	1	3	95

if these directions are perpendicular to each other, the error related to orthotropic properties will increase, which limits the use of the proposed technique. From this point of view, we made ultrasonic measurements on only one side of the AM samples.

3.3 Generalization Performance Test

The generalization performance of the pre-trained deep learning model was evaluated using newly fabricated AM samples that were not used for the training. This performance shows how the pre-trained model is generalized well for the influx of new data that is not used for model training. Therefore, the performance is used as an important index indicating the applicability of the model [15]. Three new AM samples, named T-#1, T-#2, and T-#3, were fabricated at a fixed laser power of 355 W under different laser energy densities of 55, 65, and 85 J/mm^3 (corresponding to different laser scan speeds of 1790, 1520, and 1100 mm/s), respectively. These parameters differ from the AM processing conditions for the previous twenty-four AM samples, which were used to train the deep learning model. One hundred raw ultrasonic signals in each AM sample were measured and then were input to the pre-trained model for the generalization performance test.

The results of the generalization performance test for the porosity evaluation are shown in Fig. 11. The T-#1 sample was evaluated to porosity level 0 with an 84% probability, and the next highest ranking was porosity level 1 with a 7% probability, as shown in Fig. 11a. For the T-#2 and T-#3 samples, the highest probabilities were 85% and 87% at porosity level 3 and porosity level 4, respectively. The average probability of the highest ranking in each test was 85%. Though this value was slightly lower than the testing accuracy in the previous section due to the influx of new data [46] and the difference in experimental environments [47], it was reasonably high when compared to previous studies [23].

To verify the results for porosity content evaluated by the pre-trained model, quantitative amounts of porosity contained in the newly fabricated AM samples were measured by scanning acoustic microscopy. C-scan images of the AM samples are shown in Fig. 12. The quantitative amounts of porosity content calculated from the C-scan images are

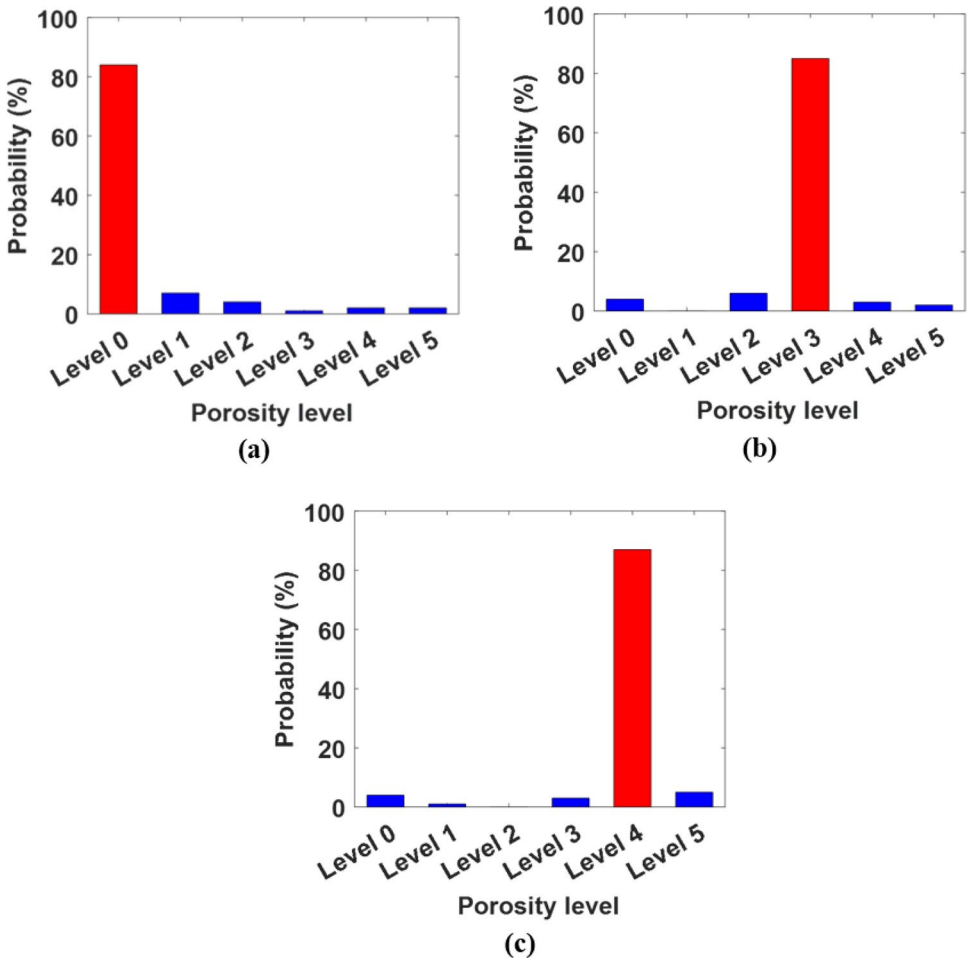

Fig. 11 The results of the generalization performance test for porosity evaluation from the **a** T-#1, **b** T-#2, and **c** T-#3 AM samples

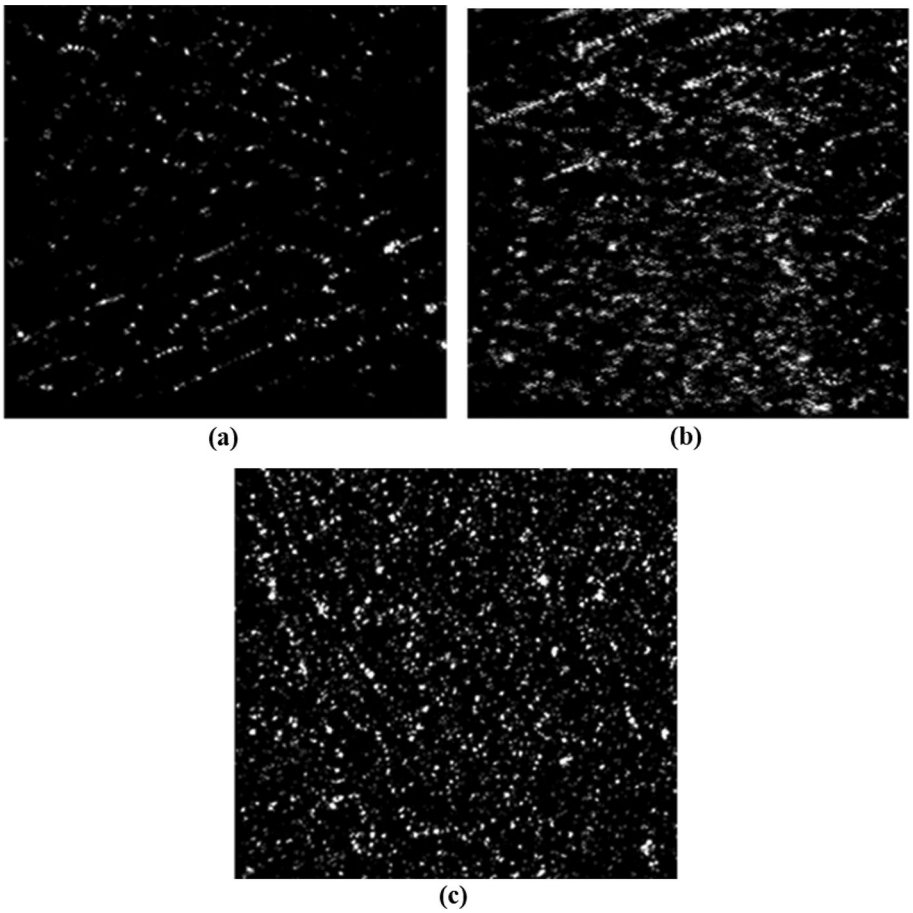

Fig. 12 C-scan images of **a** T-#1, **b** T-#2, and **c** T-#3 AM samples newly fabricated for generalization performance test

Table 6 Comparison results for porosity content evaluated by the pre-trained model and scanning acoustic microscopy

AM sample	Porosity evaluation results		
	Pre-trained model		Scanning acoustic microscopy
	Class	Porosity content (%)	Porosity content (%)
T-#1	Level 0	0–4	3.2
T-#2	Level 3	12–16	13
T-#3	Level 4	24–28	28

given in Table 6, along with the results evaluated by the pre-trained model. The measured porosity content was 3.2%, 13%, and 28% for the T-#1, T-#2, and T-#3 samples, respectively. For all three samples, the measured contents were in the range for porosity contents evaluated by the pre-trained model. In other words, the measured results were in good agreement with those of the pre-trained model, thus demonstrating that deep learning-based ultrasonic NDT could be effectively used for porosity evaluation of AM samples.

4 Conclusion

In this study, ultrasonic NDT with deep learning was proposed for porosity evaluation of AM components. This method provides (1) a porosity evaluation of AM components without conventional destructive testing owing to the direct relationship between porosity and ultrasonic properties; (2) better convenience and applicability than traditional scanning acoustic microscopy; and (3) simple ultrasonic testing using only a raw ultrasonic signal. For performance validation, porosity mechanisms with varying AM conditions were first investigated, and the fundamental correlations between porosity and ultrasonic parameters were then studied. The correlation results showed that the porosity content in AM components was highly correlated with the ultrasonic velocity and ultrasonic attenuation coefficient. Then, a deep learning model trained using ultrasonic echo signals was developed based on a fully connected DNN. The deep learning model showed an average testing accuracy of 93% for porosity evaluation. Lastly, the generalization performance of the pre-trained deep learning model was evaluated using newly fabricated AM samples that were not used for training. The results were in good agreement with the porosity contents measured via scanning acoustic

microscopy, which demonstrated the potential feasibility of deep learning-based ultrasonic NDT for porosity evaluation of AM components.

Acknowledgements This work was supported by a Korea Institute of Machinery & Materials grant funded by the Korea government (MSIT) (NK230l), and the Korea Institute of Energy Technology Evaluation and Planning (KETEP) and the Ministry of Trade, Industry and Energy (MOTIE) of the Republic of Korea (No. 20181510102360).

Compliance with Ethical Standards

Conflict of interest On behalf of all authors, the corresponding author states that there are no conflicts of interest.

References

1. Koester, L. W., Taheri, H., Bigelow, T. A., Collins, P. C., & Bonds, L. J. (2018). Nondestructive testing for metal parts fabricated using powder-based additive manufacturing. *Materials Evaluation, 76*(4), 514–524.
2. Ahn, D.-G. (2016). Direct metal additive manufacturing processes and their sustainable applications for green technology: A review. *International Journal of Precision Engineering and Manufacturing-Green Technology, 3*(4), 381–395.
3. Lee, H., Lim, C. H. J., Low, M. J., Tham, N., Murukeshan, V. M., & Kim, Y.-J. (2017). Lasers in additive manufacturing: A review. *International Journal of Precision Engineering and Manufacturing-Green Technology, 4*(3), 307–322.
4. Chua, Z. Y., Ahn, I. H., & Moon, S. K. (2017). Process monitoring and inspection systems in metal additive manufacturing: Status and applications. *International Journal of Precision Engineering and Manufacturing-Green Technology, 4*(2), 235–245.
5. Ng, G. K. L., Jarfors, A. E. W., Bi, G., & Zheng, H. Y. (2009). Porosity formation and gas bubble retention in laser metal deposition. *Applied Physics a-Materials Science & Processing, 97*(3), 641–649.
6. Eren, E., Kurama, S., & Solodov, I. (2012). Characterization of porosity and defect imaging in ceramic tile using ultrasonic inspections. *Ceramics International, 38*(3), 2145–2151.
7. Vergara, L., Miralles, R., Gosalbez, J., Juanes, F. J., Ullate, L. G., Anaya, J. J., et al. (2001). NDE ultrasonic methods to characterise the porosity of mortar. *Ndt & E International, 34*(8), 557–562.
8. Hernandez, M. G., Izquierdo, M. A. G., Ibanez, A., Anaya, J. J., & Ullate, L. G. (2000). Porosity estimation of concrete by ultrasonic NDE. *Ultrasonics, 38*(1–8), 531–533.
9. Li, W., Chen, B., Qing, X., & Cho, Y. (2019). Characterization of microstructural evolution by ultrasonic nonlinear parameters adjusted by attenuation factor. *Metals, 9*(3), 271.
10. Karthik, N. V., Gu, H., Pal, D., Starr, T., & Stucker, B. (2013). High frequency ultrasonic non destructive evaluation of additively manufactured components. *In 24th International Solid Freeform Fabrication Symposium*, 311–325.
11. Jeong, H. (1997). Effects of voids on the mechanical strength and ultrasonic attenuation of laminated composites. *Journal of Composite Materials, 31*(3), 276–292.
12. Kim, H. S., & Bush, M. B. (1999). The effects of grain size and porosity on the elastic modulus of nanocrystalline materials. *Nanostructured Materials, 11*(3), 361–367.
13. Turner, C. H., & Cowin, S. C. (1987). Dependence of elastic-constants of an anisotropic porous material upon porosity and fabric. *Journal of Materials Science, 22*(9), 3178–3184.
14. Slotwinski, J. A., Garboczi, E. J., & Hebenstreit, K. M. (2014). Porosity measurements and analysis for metal additive manufacturing process control. *Journal of Research of the National Institute of Standards and Technology, 119,* 494–528.
15. LeCun, Y., Bengio, Y., & Hinton, G. (2015). Deep learning. *Nature, 521*(7553), 436–444.
16. Nguyen, T. P., Choi, S., Park, S.-J., Park, S. H., & Yoon, J. (2020). Inspecting Method for Defective Casting Products with Convolutional Neural Network (CNN). *International Journal of Precision Engineering and Manufacturing-Green Technology*, 1–12.
17. Sambath, S., Nagaraj, P., Selvakumar, N., Arunachalam, S., & Page, T. (2010). Automatic detection of defects in ultrasonic testing using artificial neural network. *International Journal of Microstructure and Materials Properties, 5*(6), 561–574.
18. Trtnik, G., Kavcic, F., & Turk, G. (2009). Prediction of concrete strength using ultrasonic pulse velocity and artificial neural networks. *Ultrasonics, 49*(1), 53–60.
19. Harley, J. B., & Sparkman, D. (2019). Machine learning and NDE: Past, present, and future. *AIP Conference Proceedings, 2102*(1), 090001.
20. Ravanbod, H., & Jalali, A. (2008). Configurable ultrasonic flaw classification of oil pipelines. *Nondestructive Testing and Evaluation, 23*(1), 43–55.
21. Hou, W., Wei, Y., Guo, J., Jin, Y., & Zhu, C. A. (2018). Automatic detection of welding defects using deep neural network. *Journal of Physics: Conference Series, 933*(1), 012006.
22. Meng, M., Chua, Y. J., Wouterson, E., & Ong, C. P. K. (2017). Ultrasonic signal classification and imaging system for composite materials via deep convolutional neural networks. *Neurocomputing, 257,* 128–135.
23. Margrave, F. W., Rigas, K., Bradley, D. A., & Barrowcliffe, P. (1999). The use of neural networks in ultrasonic flaw detection. *Measurement, 25*(2), 143–154.
24. Yuan, S. F., Wang, L., & Peng, G. (2005). Neural network method based on a new damage signature for structural health monitoring. *Thin-Walled Structures, 43*(4), 553–563.
25. Fahad, M., Kamal, K., Zafar, T., Qayyum, R., Tariq, S., & Khan, K (2017). Corrosion detection in industrial pipes using guided acoustics and radial basis function neural network. In *International Conference on Robotics and Automation Sciences (ICRAS), IEEE*, 129–133.
26. Wang, Y., Shi, F., & Tong, X (2019). A Welding Defect Identification Approach in X-ray Images Based on Deep Convolutional Neural Networks. In *International Conference on Intelligent Computing, springer*(Cham), 53–64.
27. Isamail, L., Maskuri, N. L., Isip, N. J., Lokman, S. F., & Bakar, M. H. A. (2019). Deep Neural Network Modeling for Metallic Component Defects Using the Finite Element Model. *In Progress in Engineering Technology, springer*, 259–270.
28. Gong, H., Rafi, K., Gu, H., Starr, T., & Stucker, B. (2014). Analysis of defect generation in Ti–6Al–4V parts made using powder bed fusion additive manufacturing processes. *Additive Manufacturing, 1,* 87–98.
29. Peng, T., & Chen, C. (2018). Influence of energy density on energy demand and porosity of 316L stainless steel fabricated by selective laser melting. *International Journal of Precision Engineering and Manufacturing-Green Technology, 5*(1), 55–62.
30. Jhang, K.-Y., Choi, S., & Kim, J. (2020). Measurement of Nonlinear Ultrasonic Parameters from Higher Harmonics. *In Measurement of Nonlinear Ultrasonic Characteristics.*.
31. Kim, J., Song, D.-G., & Jhang, K.-Y. (2017). Absolute measurement and relative measurement of ultrasonic nonlinear parameters. *Research in Nondestructive Evaluation, 28*(4), 211–225.
32. Park, S.-H., Kim, J., & Jhang, K.-Y. (2017). Relative measurement of the acoustic nonlinearity parameter using laser detection of an

ultrasonic wave. *International Journal of Precision Engineering and Manufacturing, 18*(10), 1347–1352.
33. Park, S.-H., Kim, J., & Jhang, K.-Y. (2017). Measurement of absolute displacement-amplitude of ultrasonic wave using piezoelectric detection method. *Journal of the Korean Society for Nondestructive Testing, 37*(1), 7–12.
34. Jeong, H., & Hsu, D. K. (1995). Experimental-analysis of porosity-induced ultrasonic-attenuation and velocity change in carbon composites. *Ultrasonics, 33*(3), 195–203.
35. Ziółkowski, G., Chlebus, E., Szymczyk, P., & Kurzac, J. (2014). Application of X-ray CT method for discontinuity and porosity detection in 316L stainless steel parts produced with SLM technology. *Archives of Civil and Mechanical Engineering, 14*(4), 608–614.
36. Kasperovich, G., Haubrich, J., Gussone, J., & Requena, G. (2016). Correlation between porosity and processing parameters in TiAl6V4 produced by selective laser melting. *Materials & Design, 105,* 160–170.
37. Cunningham, R., Narra, S. P., Montgomery, C., Beuth, J., & Rollett, A. (2017). Synchrotron-based X-ray microtomography characterization of the effect of processing variables on porosity formation in laser power-bed additive manufacturing of Ti-6Al-4V. *JOM Journal of the Minerals Metals and Materials Society, 69*(3), 479–484.
38. Guo, C., Ge, W., & Lin, F. (2015). Effects of scanning parameters on material deposition during Electron Beam Selective Melting of Ti-6Al-4V powder. *Journal of Materials Processing Technology, 217,* 148–157.
39. Phani, K. K., & Niyogi, S. (1987). Elastic modulus-porosity relation in polycrystalline rare-earth oxides. *Journal of the American Ceramic Society, 70*(12), 362–366.
40. Zhu, K., Li, C. F., Zhu, Z. G., & Liu, C. S. (2007). Measurement of the dynamic Young's modulus of porous titanium and Ti6Al4V. *Journal of Materials Science, 42*(17), 7348–7353. https://doi.org/10.1007/s10853-007-1532-y.
41. Hirsekorn, S., Van Andel, P., & Netzelmann, U. (1998). Ultrasonic methods to detect and evaluate damage in steel. *Nondestructive Testing and Evaluation, 15*(6), 373–393.
42. Yao, X. (1999). Evolving artificial neural networks. *Proceedings of the IEEE, 87*(9), 1423–1447.
43. Aldrin, J. C., & Forsyth, D. S. (2019). Demonstration of using signal feature extraction and deep learning neural networks with ultrasonic data for detecting challenging discontinuities in composite panels. *In AIP Conference Proceedings.*
44. Tokui, S., Oono, K., Hido, S., & Clayton, J. (2015). Chainer: a next-generation open source framework for deep learning. *In Proceedings of workshop on machine learning systems (LearningSys) in the twenty-ninth annual conference on neural information processing systems (NIPS), 5*, 1–6.
45. Javidrad, H., & Salemi, S. (2020). Determination of elastic constants of additive manufactured Inconel 625 specimens using an ultrasonic technique. *International Journal of Advanced Manufacturing Technology, 107*(11–12), 4597–4607.
46. Keskar, N. S., Mudigere, D., Nocedal, J., Smelyanskiy, M., & Tang, P. T. P. (2016). On large-batch training for deep learning: Generalization gap and sharp minima. *arXiv preprint arXiv, 1609*(04836).
47. Zech, J. R., Badgeley, M. A., Liu, M., Costa, A. B., Titano, J. J., & Oermann, E. K. (2018). Variable generalization performance of a deep learning model to detect pneumonia in chest radiographs: A cross-sectional study. *Plos Medicine, 15*(11).

Seong-Hyun Park is currently a Ph.D. candidate at Hanyang University, Seoul, Korea. He received his B.S. and M.S. in mechanical engineering from Hanyang University, Seoul, Korea, in 2015 and 2017, respectively. His research interests include deep learning-based nondestructive evaluation, femtosecond laser ultrasonics, and additive manufacturing.

Sungho Choi is currently an assistant professor at Jeonbuk National University, Jeonju, Korea. He received his B.S. and Ph.D. in mechanical engineering from Hanyang University, Seoul, Korea, in 2010 and 2015, respectively. His research interests include laser-material interactions and ultrasonic nondestructive evaluation.

Kyung-Young Jhang received his B.S. and M.S. in precision mechanical engineering from Hanyang University, Seoul, Korea, in 1983 and 1985, respectively. In 1991, he received his Ph.D. in precision mechanical systems design from the Tokyo Institute of Technology, Yokohama, Japan. He has been a professor at Hanyang University, Seoul, Korea since 1992. His research interests include experimental mechanics, ultrasonic nondestructive evaluation techniques, optical measuring systems, visual image processing, random signal processing, and laser material interactions.